 © 2008 The Chemical Society of Japan

BCSJ Award Article

Mechanism and Kinetics of Cyanide Decomposition by Ferrate

Takashi Kamachi, Tomonori Nakayama, and Kazunari Yoshizawa*

Institute for Materials Chemistry and Engineering, Kyushu University, Fukuoka 819-0395

Received February 7, 2008; E-mail: kazunari@ms.ifoc.kyushu-u.ac.jp

The mechanism of cyanide oxidation by ferrate in water is discussed using DFT computations in the framework of the polarizable continuum model. The reactivity of three oxidants, nonprotonated, monoprotonated, and diprotonated ferrates is evaluated. This reaction is initiated by a direct attack of an oxo group of ferrate to the carbon atom of cyanide, followed by an H-atom transfer from cyanide to another oxo group to lead to an intermediate having cyanate (NCO^-) as a ligand. The produced cyanate is oxidized by an oxo ligand of ferrate and exogenous oxygen molecule to CO_2 and NO_2^-. The initial C–O bond formation is found to be the rate-determining step in this reaction. The activation energy for the C–O bond formation is 51.9 kJ mol^{-1} for nonprotonated ferrate, 44.4 kJ mol^{-1} for monoprotonated ferrate, and 41.4 kJ mol^{-1} for diprotonated ferrate, which indicates that the oxidizing power of the three oxidants is in the order of nonprotonated ferrate < monoprotonated ferrate < diprotonated ferrate. The general energy profile for cyanide oxidation by ferrate is downhill toward the product direction after the C–O bond formation, so cyanide is readily converted to the final products in water. The reaction kinetics of this reaction are analyzed from the calculated energy profile and experimentally determined pK_a values.

Since cyanides are used to solubilize metal ions in basic solutions, cyanide compounds are involved in wastewater streams from processes such as gold refining, metal plating, and iron and steel manufacturing.[1] The compounds are very toxic and must be removed from the wastewater prior to discharge. The most common method of cyanide destruction is alkaline chlorination using sodium hypochlorite at basic pH, as shown below.

$$NaCN + NaOCl \rightarrow NaCNO + NaCl \quad (1)$$

$$2NaCNO + 3NaOCl + H_2O \rightarrow 3NaCl + N_2 + 2NaHCO_3 \quad (2)$$

Unfortunately, this method has some disadvantages such as high chemical costs, formation of toxic intermediate, and chloride contamination. Several methods have been devised to meet growing needs for alternative methods for destroying cyanides: electrolytic decomposition, ozonation, electrodialysis, catalytic oxidation, reverse osmosis, ion exchange, genetic engineering application, and photocatalytic oxidation.[2–8]

Recently, Sharma et al.[9] reported that ferrate (FeO_4^{2-}) is an effective iron-based oxidant for cyanide destruction. This is a "green" oxidant for a variety of organic and inorganic compounds such as alcohols,[10,11] amines,[11,12] hydrazines,[13] peroxides,[14] hydrocarbons,[15] thiourea,[16] and sulfonamides[17] with harmless wastes of rust, which is easily separated from desired products. This oxidant is considerably stable in strongly alkaline solution around pH 10, whereas it decomposes spontaneously at a very rapid rate in acidic or neutral solution.[18,19] In an aqueous solution three types of ferrate coexist in equilibrium: non-protonated (tetraoxoferrate, FeO_4^{2-}), monoprotonated (hydrogentetraoxoferrate, $HFeO_4^-$), and diprotonated (tetraoxoferric acid, H_2FeO_4) ferrates.[20]

$$H_2FeO_4 \rightleftharpoons HFeO_4^- + H^+ \quad pK_1 = 3.5 \quad (3)$$

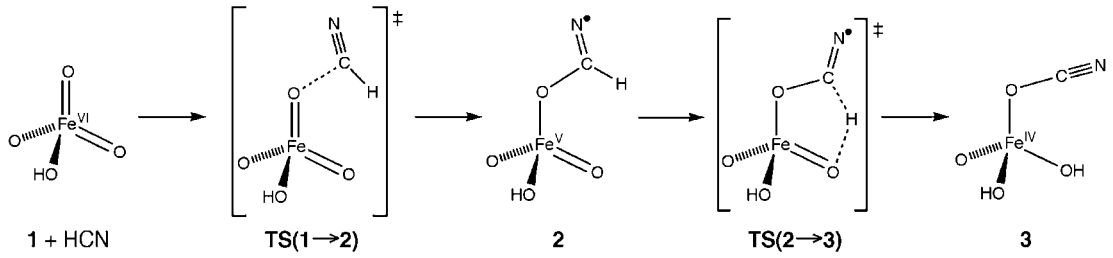
$$HFeO_4^- \rightleftharpoons FeO_4^{2-} + H^+ \quad pK_2 = 7.8 \quad (4)$$

From an X-ray analysis, ferrate was found to be tetrahedral in structure like in chromate and manganate.[21] An isotope labeling experiment of oxygen[14] and IR spectroscopy[22] demonstrated that ferrate ion remains monomeric in aqueous solution and that the four oxygen atoms of ferrate are equivalent and exchangeable with solvent water.

From density functional theory (DFT) calculations, we have investigated the mechanism and energetics of alcohol oxidation[23,24] and alkane hydroxylation[25] by ferrate. These reactions are likely to be initiated by an H-atom abstraction from a C–H or O–H bond. Our calculated results demonstrated that the oxidizing power of the three active species increases in the order nonprotonated ferrate < monoprotonated ferrate < diprotonated ferrate.[24] However, diprotonated ferrate is unlikely to be a main oxidant in the reaction because the fraction of the most active diprotonated ferrate is approximately four orders of magnitude lower than that of other ferrate species at pH 8. These results are in good agreement with experimental findings[26] that the reaction rates for alcohol oxidation are increased with the acidity of medium and that the observed pH dependence for the oxidation of 1,1,1,3,3,3-hexafluoro-2-propanol by ferrate was explained well by a kinetic model for the multi-oxidant process of FeO_4^{2-} and $HFeO_4^-$.

The destruction of cyanide by ferrate is accomplished in

Published on the web October 10, 2008; doi:10.1246/bcsj.81.1212



Scheme 1.

minutes with the formation of CO_2 and NO_2^- at pH 9.0 and 12.0.[9] The formation of cyanate ion (OCN^-) is suggested to occur in the course of this reaction, as seen in alkaline chlorination (see eq 1). This species is also observed in cyanide ozonation. Gurol and Bremen[27] reported from reaction rate measurements of cyanide ozonation that cyanate appears in the solution at a rate equal to the rate of removal of cyanide and that a direct reaction of molecular ozone contributes to cyanide destruction. We propose here a possible mechanism for cyanide destruction by ferrate from a theoretical point of view.

Method of Calculation

We calculated the energies and geometries of the reactants, intermediates, and transition states with a recently developed hybrid density functional method, the Becke88–Becke95 1-parameter model for kinetics (BB1K).[28] This method can give excellent saddle point geometries and barrier heights, and it is the best density functional method for thermochemical kinetics at present. For the Fe atom the Wachters–Hay all electron basis set (15s11p6d)/[10s7p4d][29] added by one polarization f-function ($\alpha = 1.05$)[30] was used, and for the other atoms the 6-311++G** basis set was used.[31,32] The dielectric effect of water solvent was incorporated using the polarized continuum model (PCM).[33] All geometries for reaction intermediates and transition states were fully optimized in the aqueous phase. Vibrational frequencies were systematically computed for all stationary points in order to confirm that each optimized geometry corresponds to a local minimum that has no imaginary frequency or to a saddle point that has only one imaginary frequency. Zero-point-energy corrections were taken into account for calculating the energetics of the reaction pathways. The calculated Gibbs free energies for the reaction are collected in Supporting Information. We used the Gaussian 03 ab initio program package for these calculations.[34]

Results and Discussion

Cyanate Formation. Cyanide oxidation by ferrate is expected to occur as shown in Scheme 1, in which we assume that this reaction begins with a direct attack of an oxo group to the carbon atom of cyanide in **TS(1 → 2)** to form intermediate **2**. We can rule out the occurrence of N–O bond formation in the initial step of this reaction because CNO^- lies 283.7 kJ mol^{-1} above NCO^- at the CCSD(T) level of theory.[35] After the C–O bond formation, the hydrogen atom of cyanide is abstracted by another oxo ligand via **TS(2 → 3)** to form intermediate **3** involving cyanate as a ligand.

Figure 1 shows a computed energy diagram and optimized geometries of the reaction intermediates and transition states for cyanate formation by monoprotonated ferrate. We show

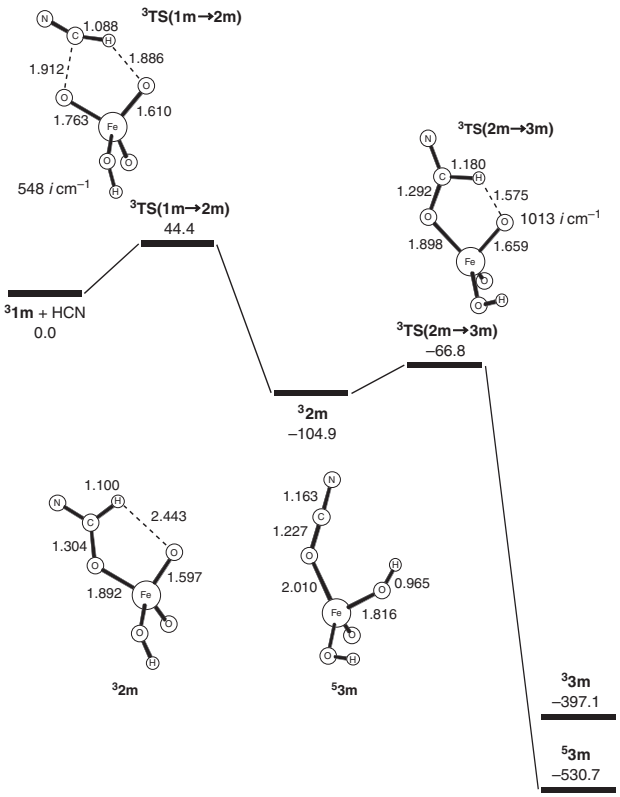


Figure 1. Energy profile (in kJ mol^{-1}) for the cyanide–cyanate conversion by mono-protonated ferrate in water. Optimized parameters are shown in Å.

in Supporting Information (Figures S1 and S2) energy diagrams for cyanate formation by non- and diprotonated ferrates. Calculated atomic charges and spin densities for these reaction species are listed in Supporting Information (Figures S3–S6). The intermediates and transition states for this reaction mediated by nonprotonated, monoprotonated, and diprotonated ferrates are labeled **n**, **m**, and **d** with numbers, respectively. The activation energy for the C–O bond formation was computed to be 44.4 kJ mol^{-1} relative to the dissociation limit. The activation barrier is 26.4 kJ mol^{-1} lower than that for the C–H bond cleavage of methanol by this oxidant,[24] indicating that cyanide is readily converted into cyanate by ferrate in water solution. The produced intermediate **2m** lies 104.9 kJ mol^{-1} below the dissociation limit and has a spin density of 1.0 on the nitrogen atom of the cyanide moiety, which indicates the reduction of the iron atom from charge VI to V. The activation energy of 38.1 kJ mol^{-1} for **TS(2m → 3m)** is 6.3 kJ mol^{-1} lower than that for **TS(1m → 2m)** and this chemical step is

Table 1. Activation Energies (kJ mol^{-1}) for the C–O Bond Formation by Nonprotonated, Monoprotonated, and Diprotonated Ferrates Using the BB1K, MPW1K, MPWB1K, B3LYP, and BP86 Methods

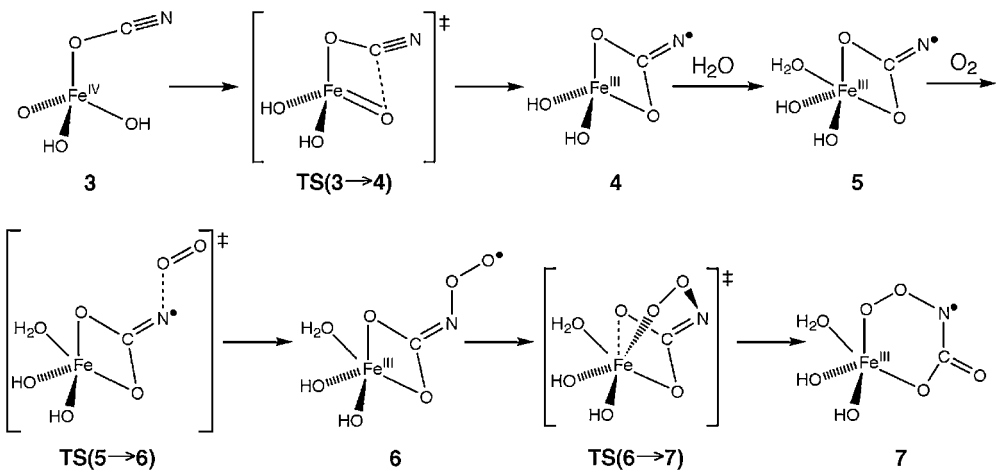
	FeO_4^{2-}	$HFeO_4^-$	H_2FeO_4
BB1K	51.9	44.4	41.4
MPW1K	44.8	20.9	20.1
MPWB1K	46.9	34.3	28.0
B3LYP	48.5	71.5	75.3
BP86	24.7	47.7	69.0

highly exothermic, suggesting that the C–O bond formation is the rate-determining step in this reaction. The spin inversion from the triplet state to the quintet state will occur in the vicinity of **3** because the high-spin states are highly preferred in tetrahedral Fe^{IV} species; the quintet state lies 133.6 kJ mol^{-1} below the triplet state.[36] We calculated the activation energies for the C–O bond formation by nonprotonated, monoprotonated, and diprotonated ferrates using the BB1K,[28] MPW1K,[37] MPWB1K,[38] B3LYP,[39,40] and BP86[39,41] methods, as listed in Table 1. The calculated barrier is sensitive to the choice of density functional. The barriers calculated with the two popular functionals, B3LYP and BP86, exhibit a clear trend: the reactivity of ferrate is decreased upon protonation. However, this result is inconsistent with experimental evidence[9] that the reaction rate for the cyanide destruction decreases nonlinearly with an increase in pH. On the other hand, the new methods developed by Lynch and Truhlar, BB1K, MPW1K, and MPWB1K correctly predict the activation energies. These functionals are optimized for a database[42] of activation energies. The estimated activation energies are in good agreement with an experimental value of 38.9 kJ mol^{-1}. To test the adequacy of the BB1K method, we considered the attack of OH radical to the carbon atom of cyanide with high-level ab initio methods. We found the BB1K method to be about as accurate for the reaction step as the CCSD(T) and MR-MP2[43] methods, as shown in Supporting Information. For these reasons, we carry out all calculations using the BB1K method in the present study.

Cyanate Oxidation. Let us next look at the reaction mechanism and energetics for cyanate oxidation by monoprotonated ferrate in water. The oxidation is initiated by the addition of the remaining oxo ligand to the carbon atom of the cyanate moiety of **3** via **TS(3 → 4)**, as shown in Scheme 2. The resultant intermediate **4** has an unpaired electron on the nitrogen atom of the cyanate moiety. The cyanate moiety is further oxidized to produce CO_2 and NO_2^-. Although the actual oxygen source for this process remains unknown, inherent oxygen molecules are proposed to be involved, as seen in the reaction of OH radicals with cyanide.[9,27] We assume that one oxygen molecule comes into the reaction system, resulting in the addition of O_2 to the radical center along this proposal. The terminal oxygen of the produced intermediate **6** coordinates to the iron atom to form a six-membered ring intermediate **7** via **TS(6 → 7)**.

Figure 2 shows a computed energy diagram and optimized geometries of the reaction intermediates and transition states for cyanate oxidation by monoprotonated ferrate. The four-centered **TS(3m → 4m)** is predicted at the C–O_{oxo} bond distance of 1.897 Å and at the Fe–O_{oxo} bond distance of 1.844 Å. The produced intermediate **4m** has a high-spin Fe^{III} oxidation state coupled with a spin-down electron on the nitrogen atom; spin densities of the Fe and N atoms are 4.3 and −1.0, respectively. We also consider another possible intermediate **4m′** produced by the attack of the oxo ligand to the nitrogen atom of the cyanate moiety. This five-membered ring intermediate lies 301.2 kJ mol^{-1} above intermediate **4m**, and therefore the mechanism involving **4m′** is ruled out. Intermediate **4m** was found to be stabilized by the coordination of one water molecule to the iron center to form intermediate **5m**.[44] The septet state lies 118.4 kJ mol^{-1} above the quintet state for the intermediate.

In the next step, one oxygen molecule comes into contact with **5m** to form an N–O bond between the nitrogen atom of **5m** and the oxygen molecule. We consider the energetics for this process along the spin septet pathway because only radicals with opposite electron spins can combine to form a covalent bond. The activation energy was computed to be 48.4 kJ mol^{-1} relative to **5m**. The electronic features of **6m** are similar to those of **5m**; for example, five unpaired electrons are localized on the Fe atom weakly coupled to an unpaired electron on the O_2 moiety of this intermediate although these electron spins are aligned in parallel. The activation energy



Scheme 2.

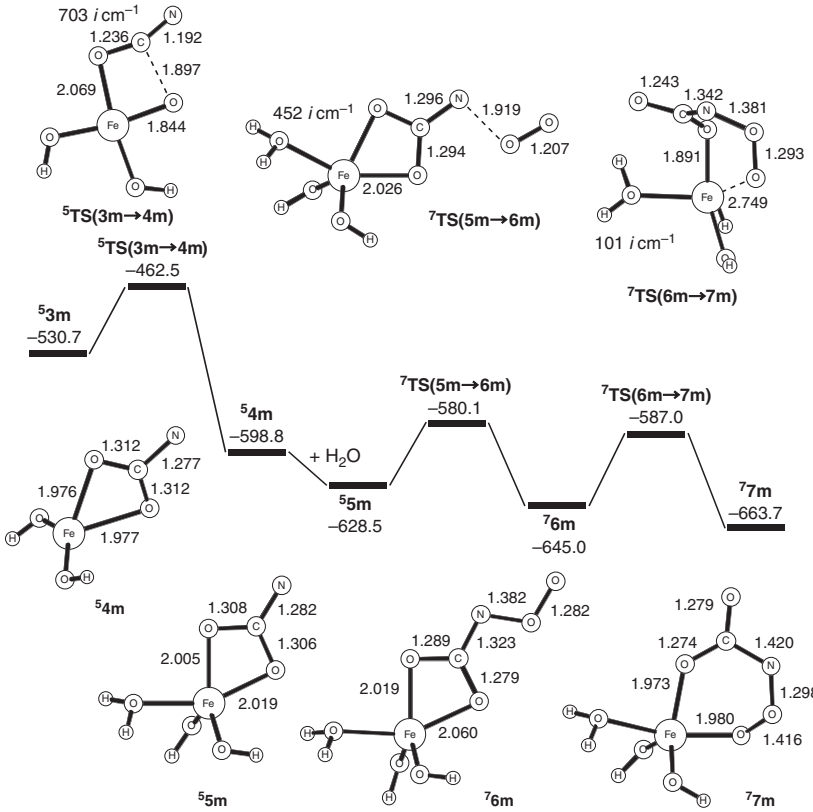
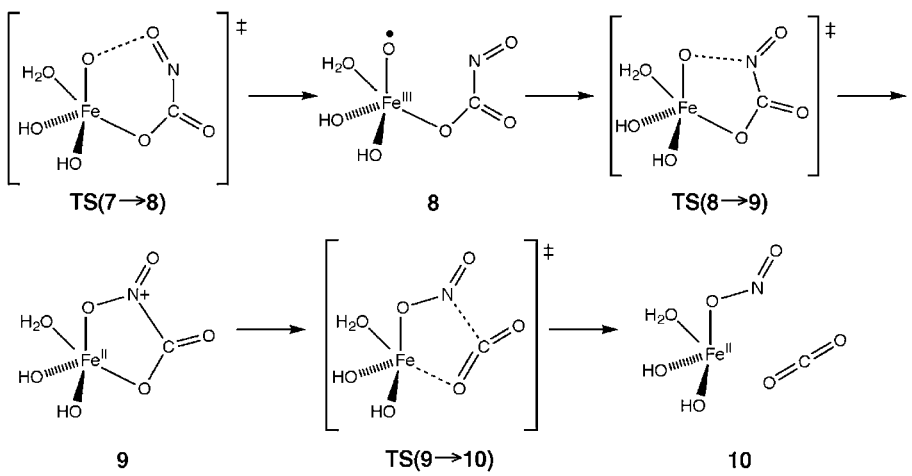


Figure 2. Energy profile (in kJ mol^{-1}) for cyanate oxidation by mono-protonated ferrate in water. Optimized parameters are shown in Å.



Scheme 3.

of **TS(6m → 7m)** was calculated to be 58.0 kJ mol^{-1} relative to **6m**. The coordination of terminal oxygen to the iron atom increases the O–O bond from 1.282 to 1.416 Å and decreases the N–O bond from 1.382 to 1.298 Å. Intermediate **7m** has a spin density of 0.7 on the nitrogen atom adjacent to the O–O bond. These geometrical and electronical structures promote the homolytic cleavage of the O–O bond, as discussed in the next section.

Production of CO_2 and NO_2^-. The destruction of cyanide by ferrate was reported to yield CO_2 and NO_2^- as final products.[9] As shown in Scheme 3, the formation of CO_2 and NO_2^- is initiated by the homolytic cleavage of the O–O bond of **7** via **TS(7 → 8)** to lead to intermediate **8** having one oxo ligand. After that, **9** is formed by the recombination of the oxo ligand and the nitrogen atom via **TS(8 → 9)**. The N–C bond of **9** is heterolytically cleaved via **TS(9 → 10)** in the final stage of the reaction. The produced CO_2 is released from the iron(II) atom in the final complex **10**. $Fe(OH)_3$ is experimentally observed as a final product, which implies that the complex **9** is oxidized by another ferrate or oxygen molecule.

Figure 3 shows a computed energy diagram and optimized geometries of the reaction intermediates and transition

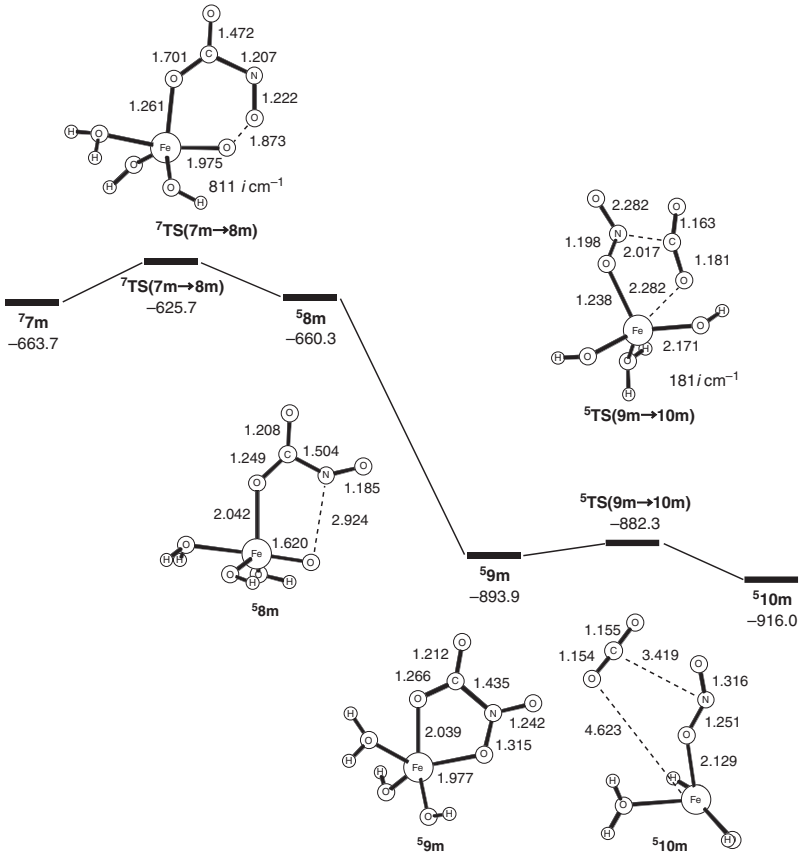


Figure 3. Energy profile (in kJ mol^{-1}) for CO_2 and NO_2^- formation by mono-protonated ferrate in water. Optimized parameters are shown in Å.

Table 2. Geometries and Energies of Points 1–7 along the Conversion Process of **^{5}8m** to **^{5}9m** in the Quintet State[a)]

	Point label						
	1	2	3	4	5	6	7
N–O	2.924	2.900	2.800	2.700	2.600	2.500	2.400
Energy	−690.5	−695.2	−696.0	−697.2	−698.5	−699.8	−701.4

a) The N–O distance is constrained during geometry optimizations. All distances and energies in the table are expressed in Å and kJ mol^{-1}, respectively.

states for CO_2 and NO_2^- formation by monoprotonated ferrate. The calculated activation energy of 38.0 kJ mol^{-1} for **TS(7m → 8m)** is rather low for the homolytic cleavage of an O–O bond: 59.8 kJ mol^{-1} for isopropenyl hydroperoxo, 60.2 kJ mol^{-1} for phenyl hydroperoxo, and 84.9 kJ mol^{-1} for an iron–hydroperoxo species of a P450 model.[45] Preliminary calculations show that the septet state lies about 83.7 kJ mol^{-1} above the quintet state in **8m**. Thus, the spin inversion from the septet state to the quintet state is likely to occur in the vicinity of **8m**. We scanned the potential energy surface of the recombination process along the N–O coordinate, as listed in Table 2. Starting from **8m** (point 1), we obtained the structure of points 2–7 by partial optimizations under the constraint of the N–O distance. This calculational result strongly suggests that **8m** will collapse into **9m** virtually in a barrierless manner; in fact, detailed transition-state searches failed to precisely locate such a transition state. The N–C bond of 1.435 Å in **9m** is cleaved via **TS(9m → 10m)** to give rise to **10m**, in which CO_2 and NO_2^- coordinate to the iron atom. The spin densities on the CO_2 and NO_2 moiety of **TS(9m → 10m)** were calculated to be almost zero. This result demonstrates that the N–C bond dissociation should take place in a heterolytic manner. The overall conversion of cyanide to CO_2 and NO_2^- is exothermic by 916.0 kJ mol^{-1} and the transition states involved in the reaction are low-lying after the initial C–O bond formation, and therefore, this reaction should easily take place in water.

Kinetics of Cyanide Destruction. Let us finally look at the reaction kinetics using the information on the obtained potential energy diagrams to refine the reaction mechanism. Our calculated results show that the activation energy for cyanide destruction is decreased upon protonation of ferrate, as seen in alcohol oxidation.[23,24] However, diprotonated ferrate is unlikely to be involved as a main oxidant in the reaction because this highly reactive species exists in aqueous solution in extremely small quantities under experimental conditions. To clarify the relationship between the concentration and reactivity of these species, we estimated the net rate of cyanide destruction by ferrate with the following expression:

$$-\mathrm{d[M]}/\mathrm{d}t = k_\mathrm{n}[\mathrm{FeO_4}^{2-}][\mathrm{M}] + k_\mathrm{m}[\mathrm{HFeO_4}^{-}][\mathrm{M}] + k_\mathrm{d}[\mathrm{H_2FeO_4}][\mathrm{M}] \quad (5)$$

where [M] is the concentration of cyanide and k_n, k_m, and k_d are the reaction rate constants for FeO_4^{2-}, $HFeO_4^-$, and H_2FeO_4, respectively. We assumed that the rate law for each

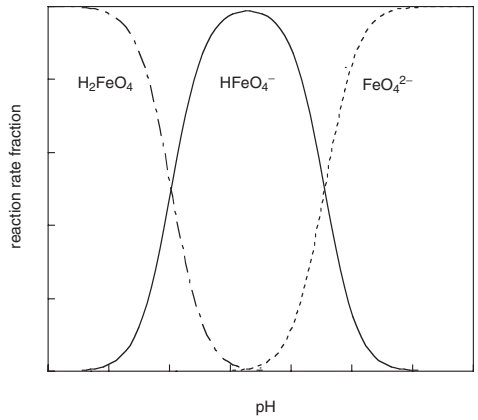


Figure 4. Estimated reaction rate fraction of FeO_4^{2-}, $HFeO_4^-$, and H_2FeO_4 in water as a function of pH.

pathway is first order with respect to the concentration of oxidant and cyanide because this reaction is downhill and highly exothermic without high barriers after the initial C–O bond formation. Mono- and diprotonation of FeO_4^{2-} reduce the activation barriers for the C–O bond formation by 7.5 and 10.5 kJ mol^{-1}, respectively, which leads to an acceleration of the reaction rate ($k_m/k_n = 20.86$ and $k_d/k_n = 67.99$). We estimated the pH dependence of concentration of these three oxidants using eqs 3 and 4.[46] Figure 4 shows calculated relative reaction rates of FeO_4^{2-}, $HFeO_4^-$, and H_2FeO_4 in water as a function of pH at 300 K. This diagram is similar to the one given in previous work.[47] This result clearly demonstrates that the identity of the main oxidant for the reaction is dependent on pH; FeO_4^{2-} in pH of 10–14, $HFeO_4^-$ in pH of 5–8, and H_2FeO_4 in pH of 0–3. The reaction rates are too fast to be measured at pH lower than 8.0 and a higher amount of ferrate needs to be used for complete removal of cyanide at pH 7.5.[9] This would be ascribed to the decomposition of $HFeO_4^-$ in the neutral solution. Sharma et al.[9] demonstrated that the molar consumption of ferrate is nearly equal to that of oxidized cyanide and that the oxidant has a maximum efficiency for removing cyanide at pH 9.0.[9] Our calculational results show that the identity of the main oxidant for the reactions is dependent on pH and that the two oxidants, FeO_4^{2-} and $HFeO_4^-$, compete for cyanide destruction at the pH optimum condition (44% for FeO_4^{2-}, 56% for $HFeO_4^-$).

Conclusion

We elucidated the mechanism of cyanide oxidation by ferrate in water from DFT computations. This reaction starts from the formation of a C–O bond between the oxo group of ferrate and the carbon atom of cyanide, followed by the cleavage of the C–H bond of cyanide by another oxo group. The resultant intermediate has cyanate (NCO^-) as a ligand, which is consistent with an experimental result that this ion is detected as a by-product. The produced cyanate is further oxidized by an oxo ligand of ferrate and exogenous molecular oxygen to CO_2 and NO_2^-. Our calculations indicate that spin inversions are likely to take place in the course of the reaction. The overall conversion of cyanide to CO_2 and NO_2^- is highly exothermic and the transition states involved are relatively low-lying after the initial C–O bond formation, and therefore, the C–O bond formation is the rate-determining step in this reaction. We evaluated the activation energy for the first step mediated by three kinds of oxidants, FeO_4^{2-}, $HFeO_4^-$, and H_2FeO_4, using the BB1K method. The oxidizing power of the three active species is found to increase in the order of non-protonated ferrate < monoprotonated ferrate < diprotonated ferrate. We have analyzed the pH dependence of this reaction using a simple kinetics model. The calculated relative reaction rate of cyanide destruction by ferrate shows that FeO_4^{2-} and $HFeO_4^-$ compete in this reaction at pH 9.0 and 300 K.

T.K. acknowledges a Grant-in-Aid (No. 18750048) for Young Scientists B from Japan Society for the Promotion of Science (JSPS). K.Y. acknowledges Grants-in-Aid (Nos. 18350088, 18GS0207, and 18066013) for Scientific Research from JSPS and the Ministry of Education, Culture, Sports, Science and Technology of Japan (MEXT), the Nanotechnology Support Project of MEXT, the Joint Project of Chemical Synthesis Core Research Institutions of MEXT, and CREST of Japan Science and Technology Cooperation for their support of this work. We are thankful to Professor V. K. Sharma for his kind advice and discussion.

Supporting Information

Two figures of energy diagrams for the cyanate formation by non- and diprotonated ferrates, four figures of calculated atomic charges and spin densities of all reaction species, 31 tables for optimized geometries of all the reaction species, one table for the triplet–quintet energy separation for **3m**, one table for the attack of OH radical to HCN, and one table for calculated Gibbs free energies for the reaction. These materials are available free of charge on the web at http://www.csj.jp/journals/bcsj/.

References

1 P. Gallerani, D. Drake, *Plat. Surf. Finish.* **1993**, *80*, 28.
2 J. A. Zeevalkink, D. C. Visser, P. Arnoldy, C. Boelhouwer, *Water Res.* **1980**, *14*, 1375.
3 S. Basheer, O. M. Kut, J. E. Prenosil, J. R. Bourne, *Biotechnol. Bioeng.* **1992**, *39*, 629.
4 Y. Chen, C. You, W. Ying, *Met. Finish.* **1991**, *89*, 68.
5 M. Futakawa, H. Takahashi, G. Inoue, T. Fujioka, *Desalination* **1994**, *98*, 345.
6 J. Hwang, Y. Wang, C. Wang, *J. Appl. Electrochem.* **1987**, *17*, 684.
7 D. Bhakta, S. S. Shukla, M. S. Chandrasekharalah, J. L. Margrave, *Environ. Sci. Technol.* **1992**, *26*, 625.
8 C. H. Pollema, J. L. Hendrix, E. B. Milosavljevic, L. Solujic, J. H. Nelson, *J. Photochem. Photobiol.* **1992**, *66*, 235.
9 V. K. Sharma, W. Rivera, J. O. Smith, B. O'Brien, *Environ. Sci. Technol.* **1998**, *32*, 2608.
10 R. J. Audette, J. W. Quail, P. J. Smith, *Tetrahedron Lett.* **1971**, *12*, 279.
11 Y. Tsuda, S. Nakajima, *Chem. Lett.* **1978**, 1397.
12 M. D. Johnson, B. J. Hornstein, *Inorg. Chem.* **2003**, *42*, 6923.
13 M. D. Johnson, B. J. Hornstein, *Inorg. Chim. Acta* **1994**, *225*, 145.
14 H. Goff, R. K. Murmann, *J. Am. Chem. Soc.* **1971**, *93*, 6058.
15 L. Delaude, P. Laszlo, *J. Org. Chem.* **1996**, *61*, 6360.

16 V. K. Sharma, W. Rivera, V. N. Joshi, F. J. Millero, D. O'Connor, *Environ. Sci. Technol.* **1999**, *33*, 2645.

17 V. K. Sharma, S. K. Mishra, N. Nesnas, *Environ. Sci. Technol.* **2006**, *40*, 7222.

18 W. F. Wagner, J. R. Gump, E. N. Hart, *Anal. Chem.* **1952**, *24*, 1497.

19 R. H. Wood, *J. Am. Chem. Soc.* **1958**, *80*, 2038.

20 J. D. Carr, P. B. Kelter, A. Tabatabai, D. Spichal, J. Erickson, C. W. McLaughlin, Proceedings of the Conference on Water Chlorination and Chemical Environment Impact Health Effects, **1985**.

21 M. L. Hoppe, E. O. Schlemper, R. K. Murmann, *Acta Crystallogr., Sect. B* **1982**, *38*, 2237.

22 W. P. Griffith, *J. Chem. Soc. A* **1966**, 1467.

23 T. Ohta, T. Kamachi, Y. Shiota, K. Yoshizawa, *J. Org. Chem.* **2001**, *66*, 4122.

24 T. Kamachi, T. Kouno, K. Yoshizawa, *J. Org. Chem.* **2005**, *70*, 4380.

25 Y. Shiota, N. Kihara, T. Kamachi, K. Yoshizawa, *J. Org. Chem.* **2003**, *68*, 3958.

26 B. E. Norcross, W. C. Lewis, H. Gai, N. A. Noureldin, D. G. Lee, *Can. J. Chem.* **1997**, *75*, 129.

27 M. D. Gurol, W. M. Bremen, *Environ. Sci. Technol.* **1985**, *19*, 804.

28 Y. Zhao, B. J. Lynch, D. G. Truhlar, *J. Phys. Chem. A* **2004**, *108*, 2715.

29 a) A. J. H. Wachters, *J. Chem. Phys.* **1970**, *52*, 1033. b) P. J. Hay, *J. Chem. Phys.* **1977**, *66*, 4377.

30 K. Raghavachari, G. W. Trucks, *J. Chem. Phys.* **1989**, *91*, 1062.

31 R. Krishnan, J. S. Binkley, R. Seegar, J. A. Pople, *J. Chem. Phys.* **1980**, *72*, 650.

32 T. Clark, J. Chandrasekhar, G. W. Spitznagel, P. v. R. Schleyer, *J. Comput. Chem.* **1983**, *4*, 294.

33 a) S. Mierts, E. Scrocco, J. Tomasi, *Chem. Phys.* **1981**, *55*, 117. b) S. Miertus, J. Tomasi, *Chem. Phys.* **1982**, *65*, 239. c) V. Barone, M. Cossi, J. Tomasi, *J. Chem. Phys.* **1997**, *107*, 3210. d) M. Cossi, V. Barone, R. Cammi, J. Tomasi, *Chem. Phys. Lett.* **1996**, *255*, 327.

34 M. J. Frisch, G. W. Trucks, H. B. Schlegel, G. E. Scuseria, M. A. Robb, J. R. Cheeseman, J. A. Montgomery, Jr., T. Vreven, K. N. Kudin, J. C. Burant, J. M. Millam, S. S. Iyengar, J. Tomasi, V. Barone, B. Mennucci, M. Cossi, G. Scalmani, N. Rega, G. A. Petersson, H. Nakatsuji, M. Hada, M. Ehara, K. Toyota, R. Fukuda, J. Hasegawa, M. Ishida, T. Nakajima, Y. Honda, O. Kitao, H. Nakai, M. Klene, X. Li, J. E. Knox, H. P. Hratchian, J. B. Cross, V. Bakken, C. Adamo, J. Jaramillo, R. Gomperts, R. E. Stratmann, O. Yazyev, A. J. Austin, R. Cammi, C. Pomelli, J. W. Ochterski, P. Y. Ayala, K. Morokuma, G. A. Voth, P. Salvador, J. J. Dannenberg, V. G. Zakrzewski, S. Dapprich, A. D. Daniels, M. C. Strain, O. Farkas, D. K. Malick, A. D. Rabuck, K. Raghavachari, J. B. Foresman, J. V. Ortiz, Q. Cui, A. G. Baboul, S. Clifford, J. Cioslowski, B. B. Stefanov, G. Liu, A. Liashenko, P. Piskorz, I. Komaromi, R. L. Martin, D. J. Fox, T. Keith, M. A. Al-Laham, C. Y. Peng, A. Nanayakkara, M. Challacombe, P. M. W. Gill, B. Johnson, W. Chen, M. W. Wong, C. Gonzalez, J. A. Pople, *Gaussian 03, Revision B. 03*, Gaussian, Inc., Wallingford CT, 2004.

35 Y. Pak, R. C. Woods, K. A. Peterson, *J. Chem. Phys.* **1997**, *106*, 5123.

36 The BB1K functional is particularly robust for predicting the triplet–quintet energy separation for this species. See Table S32 in Supporting Information.

37 B. J. Lynch, P. L. Fast, M. Harris, D. G. Truhlar, *J. Phys. Chem. A* **2000**, *104*, 4811.

38 Y. Zhao, D. G. Truhlar, *J. Phys. Chem. A* **2004**, *108*, 6908.

39 a) A. D. Becke, *Phys. Rev. A* **1988**, *38*, 3098. b) A. D. Becke, *J. Chem. Phys.* **1993**, *98*, 5648.

40 C. Lee, W. Yang, R. G. Parr, *Phys. Rev. B* **1988**, *37*, 785.

41 J. P. Perdew, *Phys. Rev. B* **1986**, *33*, 8822.

42 B. J. Lynch, D. G. Truhlar, *J. Phys. Chem. A* **2003**, *107*, 8996.

43 a) H. Nakano, *Chem. Phys. Lett.* **1993**, *207*, 372. b) H. Nakano, *J. Chem. Phys.* **1993**, *99*, 7983.

44 F. P. Rotzinger, *J. Phys. Chem. B* **2005**, *109*, 1510.

45 R. D. Bach, O. Dmitrenko, *J. Am. Chem. Soc.* **2006**, *128*, 1474.

46 We calculated the reaction rate fraction of FeO_4^{2-} with the following equation

$$\frac{k_n[FeO_4^{2-}]}{k_n[FeO_4^{2-}] + k_m[HFeO_4^{-}] + k_d[H_2FeO_4]}$$

and the concentration of the three oxidants was determined with eqs 3 and 4.

47 V. K. Sharma, *Adv. Environ. Res.* **2002**, *6*, 143.